Reduced grid-like theta modulation in schizophrenia

Laura Convertino,[1,2,†] Daniel Bush,[3,†] Fanfan Zheng,[4] Rick A. Adams[1,2,5,6,7] and Neil Burgess[1,2,8]

[†]**These authors contributed equally to this work.**

Abstract

The hippocampal formation has been implicated in the pathophysiology of schizophrenia, with patients showing impairments in spatial and relational cognition, structural changes in entorhinal cortex, and reduced theta coherence with medial prefrontal cortex. Both the entorhinal cortex and medial prefrontal cortex exhibit a six-fold (or 'hexadirectional') modulation of neural activity during virtual navigation that is indicative of grid cell populations and associated with accurate spatial navigation.

Here, we examined whether these grid-like patterns are disrupted in schizophrenia. We asked 17 participants with diagnoses of schizophrenia and 23 controls (matched for age, sex and IQ) to perform a virtual reality spatial navigation task during magnetoencephalography.

The control group showed stronger 4-10 Hz theta power during movement onset, as well as hexadirectional modulation of theta band oscillatory activity in the right entorhinal cortex whose directional stability across trials correlated with navigational accuracy. This hexadirectional modulation was absent in patients, with a significant difference between groups.

These results suggest that impairments in spatial and relational cognition associated with schizophrenia may arise from disrupted grid firing patterns in entorhinal cortex.

Author affiliations:

1 Institute of Cognitive Neuroscience, University College London, London, UK

2 Wellcome Centre for Human Neuroimaging, University College London, London, UK

3 Department of Neuroscience, Physiology and Pharmacology, University College London, London, UK

4 School of Nursing, Peking Union Medical College, Chinese Academy of Medical Sciences, Beijing, China

5 Division of Psychiatry, University College London, London, UK

6 Max Planck-UCL Centre for Computational Psychiatry and Ageing Research, London, UK

7 Centre for Medical Image Computing, Department of Computer Science, University College London, London, UK

8 Queen Square Institute of Neurology, University College London, London, UK

Correspondence to: Prof. Neil Burgess

UCL Institute of Cognitive Neuroscience, Alexandra House, 17 Queen Square, London WC1N 3AZ

E-mail: n.burgess@ucl.ac.uk

Running title: Reduced grid-like theta in schizophrenia

Keywords: schizophrenia; entorhinal cortex; grid cells; spatial memory

Abbreviations: BOLD = blood oxygen level dependent; fMRI = functional magnetic resonance imaging; MEG = magnetoencephalography; mPFC = medial prefrontal cortex; MTL = medial temporal lobe; MNI = Montreal Neurological Institute; ROI = region of interest; VR = virtual reality

Introduction

Schizophrenia is characterised by distortion of thoughts and perception including delusions, hallucinations, disorganised or catatonic behaviour, and diminished emotional expression or motivation (DSM-5, 2013). Several studies suggest a role for the hippocampal formation in the pathophysiology of schizophrenia[1-5]. Specifically, patients exhibit structural changes in entorhinal cortex[6-8] and reduced functional connectivity between the medial temporal lobe

(MTL) and medial prefrontal cortex (mPFC)[1,9-12]. The hippocampal formation plays a fundamental role in episodic memory and spatial navigation[13,14]. Consistent with this, patients with schizophrenia also exhibit impaired performance in a range of spatial navigation tasks[15-19].

Spatial cognition appears to depend on specialised populations of neurons including grid cells[20], originally identified in the rodent medial entorhinal cortex and subsequently found in the human entorhinal cortex and mPFC[21]. Grid cells exhibit periodic spatial firing fields with six-fold (or 'hexadirectional') rotational symmetry. Grid cells are thought to support accurate spatial navigation[22-24] and may also contribute to relational memory[25,26] and the acquisition of structural knowledge[27]. Hence, we examined whether grid cell activity patterns might be disrupted in schizophrenia.

In rodents, grid cell firing patterns appear to depend on movement-related theta band oscillations[28-30]. There is also evidence for movement-related theta oscillations in human intracranial local field potentials[31-33], particularly during movement initiation[34]. Hexadirectional modulation of theta band activity, consistent with the presence of grid cell firing patterns, has also been observed in intracranial EEG recordings from the entorhinal cortex during virtual navigation[35,36], building on observations of similar patterns in BOLD signal throughout the default mode network[37]. We therefore asked participants with a diagnosis of schizophrenia (half of whom were unmedicated) and a matched control group to complete an established spatial navigation task inside a magnetoencephalography (MEG) scanner[1,38,39]. We then looked for hexadirectional modulation of theta band oscillatory activity during virtual movement.

Materials and methods

Participants

This study re-analyses MEG data first presented in[1]. The study was approved by the local NHS research ethics board (REF: 17/LO/0027), and all participants gave informed consent. Age, sex, IQ, digit span, handedness, and years in education information was collected from all participants. Participants with a schizophrenia diagnosis also completed the Positive and Negative Symptoms Scale[40], a saliva recreational drugs test (see Supplementary Table 1 in[1]), and documented their medication. To be included, participants must have been educated in English,

not be using benzodiazepines or anticonvulsants, have normal (or corrected to normal) vision, and be under 60 years old. The patient group was recruited based on DSM-IV criteria for schizophrenia, with 18 participants in total. Patients had no other psychiatric diagnoses, based on the structured clinical interview for DSM-IV-TR axis I disorders[41]. The control group were recruited to match the age, sex, and IQ of the patient group as closely as possible, with 35 participants in total. Controls were excluded if they had history of a psychiatric or neurological condition. In addition, one patient and twelve control participants were excluded due to excessive MEG artefacts, interruption of the experiment due to nausea or sleep, or loss of fiducial markers. This left 17 patients (14 males) and 23 controls (17 males). All participants were asked not to consume caffeine or smoke on the testing day.

Spatial memory task

Inside the MEG scanner, participants performed a spatial memory task in a virtual reality environment[42] constructed using the Unity game engine (Unity Technologies Ltd). During the task, participants navigated freely around up to three different virtual reality environments and were asked to learn – and subsequently recall – the locations of four different objects in each environment (Fig. 1A). Movement was directed using three buttons controlling left and right rotation and forward translation (via rapid acceleration to a fixed maximum speed). The environments were 100 virtual metre (vm) square arenas delineated by a solid boundary and surrounded by distant landmarks. Each environment was distinguished by the surface textures used for the floor and boundary, the location and identity of distal cues, and the location and identity of the objects being memorised. At the start of each block (in each different environment), participants were placed in the centre of the environment facing in the same direction (north).

During encoding, one of four objects was visible in the environment in each trial, and participants were instructed to remember the location of that object. Once they were happy that they had remembered its location, they collided with the object to move to the next trial. There were two encoding trials for each object, in a pseudorandom order, giving eight encoding trials in each environment. Object locations were selected from 16 possible locations, so that each environment contained two objects close to the middle of the arena, one close to a corner and one

near the middle of a boundary, to match difficulty across environments (with object locations not used more than once across environments).

During retrieval, each trial began with a 3 s fixation cross, followed by a 3 s cue period in which a single target object was presented on screen. Participants were then placed at a random location and orientation within the environment and asked to navigate to the location of that object and make a button press response. Participants subsequently received feedback on their performance, i.e. the cued object appeared in its correct location, and the next trial began when they collided with the object. Performance in each trial was quantified using the inverse of the distance between the remembered object location and its actual location (such that larger values correspond to better performance, as used in[37]). There were eight retrieval trials for each object, giving 32 retrieval trials in each environment. Controls and patients completed 2.70 ± 0.56 and 2.88 ± 0.33 (mean ± SD) task blocks (i.e. environments), respectively.

MEG data collection and pre-processing

MEG data were acquired using a 275-channel axial gradiometer system (CTF Omega, VSM MedTech) at a sample rate of 480 Hz. During the recording, head position coils (attached to nasion and left and right pre-auricular sites) were used for anatomical co-registration, and eye tracking was performed using an Eyelink 1000 system (SR Research). Raw MEG data were imported into SPM12[43] and downsampled to 200 Hz before eye blink and heartbeat artefacts were manually identified and removed using ICA implemented in FieldTrip[44] and EEGLAB[45]. Finally, a fifth order, zero phase Butterworth filter was used to remove slow drift (1 Hz high-pass) and mains noise (48-52 Hz notch) from the recordings.

Our analyses focussed on periods of movement onset and complete immobility in the virtual environment. Movement onset 'epochs' were defined as [-3 3] s windows around the onset of continuous translational movements that lasted ≥1 s and were preceded by ≥1 s of complete immobility (consistent with previous studies[34]). This captured 25.4 ± 6.9% and 25.5 ± 6.4% of the task data for controls and patients, respectively. Stationary 'epochs' were defined as [-2.5 3.5] s windows around the onset of ≥2 s periods during which no translational movement occurred. This captured 51.4 ± 8.9% and 49.8 ± 7.2% of the task data for controls and patients, respectively (see Table 1 for trial numbers). Importantly, although these epochs could overlap,

the overlapping time periods were not included in any of our analyses (see Supplementary Fig. 1 and further details below). Once the MEG data had been divided into movement onset and stationary epochs, artefact trials were automatically identified and removed using an underlying outlier test (with a threshold of α=0.05).

MEG data analysis

To examine changes in low frequency power associated with the onset of virtual movement, we generated a time frequency spectrogram for each movement and stationary period in the 2-70 Hz range using a five cycle Morlet wavelet transform for 40 equally logarithmically spaced frequencies. The resulting power values were log transformed and normalised by the sum of power values across frequencies at each time point. Finally, power values were averaged across epochs for each participant, and power in the [-0.5 0.5] s window around movement onset was baseline corrected by average power in the [0 1] s window during stationary periods. Inspection of the resultant power spectrum, averaged across all participants in both groups, revealed a peak in the 4-10 Hz theta band on which subsequent analyses were focussed. Source localisation of 4-10 Hz theta power was performed in SPM12 using the Linearly Constrained Minimum Variance beamformer from the DAiSS toolbox, with a single-shell forward model and sources evenly distributed on a 10mm grid co-registered to MNI coordinates. This resulted in a set of linear weights for each participant that could generate 4-10 Hz band-pass filtered time series in source space from sensor-level data in each movement onset epoch[46].

To look for the hexadirectional modulation of theta power, we first isolated the continuous period of translational movement following movement onset in each epoch. Next, for each task block (i.e. each virtual environment), we extracted continuous movement direction from the corresponding behavioural data and a measure of theta power by applying the Hilbert transform to band-pass filtered data in each voxel and Z-scoring the resultant time series (to match signal amplitude across voxels and participants). We then estimated grid orientation independently for each voxel using a quadrature filter[37] applied to alternate movement onset epochs from that block. Finally, we estimated the strength of hexadirectional modulation in each voxel for the remaining movement onset epochs by linearly regressing continuous theta power against the cosine of the angular deviation from that grid orientation, with six-fold periodicity (see

Supplementary Fig. 2 for a schematic). We repeated this analysis, reversing the use of alternate epochs for estimating orientation and modulation, and averaged the regression coefficients across the two folds and then across task blocks to provide a single metric indicating the strength of hexadirectional theta modulation for each participant in each voxel. The same analysis was also performed for other rotational symmetries (specifically: four-, five-, seven-, and eight-fold) and hexadirectional modulation in other oscillatory bands (specifically: 2-4 Hz delta, 12-20 Hz alpha, 20-35 Hz beta and 40-70 Hz gamma). For anatomically defined region of interest (ROI) analyses, we used probabilistic masks from the Julich-Brain Cytoarchitectonic Atlas[47] thresholded at a probability value of 40%.

Data availability

The data and custom written analysis code that support the findings of this study are available on request from the corresponding author.

Results

We asked participants with a diagnosis of schizophrenia (half of whom were unmedicated) and an age, sex and IQ matched control group to perform an established spatial navigation task[1,38,39,42] using desktop virtual reality (VR) inside a magnetoencephalography (MEG) scanner (Fig. 1A). Consistent with previous reports[15-19], spatial memory performance was significantly better in the control group ($t(38)=2.10$, $p=0.042$, Hedge's $g=0.66$, *CI* [0.028 1.32]; Fig. 1B).

To look for evidence of grid-like activity during translational movement within the VR environment, we first investigated changes in oscillatory power associated with movement onset versus stationary periods. Power spectra for both groups, averaged across all sensors, showed a peak in the theta band during movement onset (Fig. 2A). Specifically, 4-10 Hz theta power was greater during movement onset than stationary periods in both controls ($t(22)=5.58$, $p<0.001$) and patients ($t(16)=2.39$, $p=0.03$), and greater in controls than patients ($t(38)=2.02$, $p=0.05$, $g=0.63$, *CI* [0.0014 1.29]; Supplementary Fig. 3A). This is illustrated by time-frequency spectrograms of movement onset periods (Fig. 2B), which show a clear increase in theta power

in the control group beginning ~0.5 s prior to movement onset (consistent with previous reports[34,39]) that is markedly reduced in patients.

Scalp plots (showing normalised power differences between movement onset and stationary periods) illustrate that 4-10 Hz theta power increases arise over bilateral frontal and temporal sensors in both groups, with controls showing greater movement-related theta power than patients over left frontal sensors (Fig. 2C). Importantly, we found no evidence for differences in movement statistics between control and patient groups in the virtual environment that could account for these differences. Specifically, there were no differences in the average duration of movements between patients (mean ± SD = 2.29 ± 0.43 s) and controls (2.18 ± 0.5 s; $t(38)=-0.723$, $p=0.47$) or preference to navigate close to the boundaries of the environment (patients: 79.2 ± 4.8%; controls: 79.9 ± 6.1%; $t(38)=0.37$, $p=0.71$), and movement speed accelerated rapidly to a fixed top speed for all participants.

Next, we looked for hexadirectional modulation of movement-related theta power across the whole brain using established methods[37] (see Supplementary Fig. 2 for further details). Remarkably, the control group showed a single significant cluster of hexadirectional theta modulation in the vicinity of right entorhinal cortex (Fig. 3A). In contrast, the patient group showed no clusters that passed our threshold of $p<0.05$ FWE corrected across the whole brain.

To further characterise this effect, we extracted the strength and orientation of hexadirectional theta power modulation from each voxel in an anatomically-defined right entorhinal region of interest (ROI) for each participant (Fig. 3B). Consistent with the whole brain results, this revealed significant hexadirectional modulation of 4-10 Hz theta power for controls ($t(22)=3.04$, $p=0.0059$) but not patients ($t(16)=-0.04$, $p=0.97$), and significantly stronger hexadirectional modulation for controls than patients ($t(38)=2.08$, $p=0.044$, $g=0.65$, CI [0.02 1.31]; Fig. 3C). Similarly, theta power in this ROI was greater during movement aligned versus misaligned with the grid axes for controls (i.e. within ±15° of the fitted grid orientation versus other movement directions; $t(22)=2.82$, $p=0.01$; Fig. 3D), despite no difference in the proportion of movement samples with aligned versus misaligned directions ($t(22)=-0.70$, $p=0.49$; Fig. 3E). Importantly, theta power from this ROI was not significantly modulated by four, five, seven or eight fold movement direction in the control group (although we note a trend towards significance for eight-fold modulation ($t(22)=2.03$, $p=0.055$; all others $p>0.27$; Fig. 3F), nor was there any

evidence for hexadirectional modulation of delta, alpha, beta, or gamma frequency band activity in this region (all $p>0.26$; Fig. 3G). In addition, we found no evidence for the hexadirectional modulation of theta power within a corresponding anatomically-defined left entorhinal ROI (Supplementary Fig. 3B).

Reassuringly, grid orientation across voxels inside the right entorhinal ROI (within each task block and data partition) was more consistent than expected by chance (5.33 ± 2.25°, chance=15°; $t(22)=-20.7$, $p<0.001$), as was grid orientation across data partitions, each including half of the trials (within each task block and ROI voxel; 12.9 ± 3.55°; $t(22)=-2.85$, p=0.0093). However, grid orientation across blocks (within each data partition and voxel inside the ROI) was no more consistent than expected by chance (15.5 ± 3.05°, $t(21)=0.71$, $p=0.49$), suggesting that grid patterns randomly realigned with the visually distinct square environment encountered in each task block. Importantly, we found no evidence for a relationship between theta power during movement onset (averaged across all sensors) and the strength of hexadirectional modulation inside the ROI (Pearson's $r=0.32$, $p=0.14$); or between theta power during movement onset (averaged across all voxels within the ROI) and the strength of hexadirectional modulation in the same region ($r=0.25$, $p=0.25$). This suggests that differences in the magnitude of hexadirectional modulation across participants did not arise simply from differences in the power of the underlying theta oscillation.

Finally, we looked for a relationship between the hexadirectional modulation of 4-10 Hz theta power inside the ROI and our behavioural data. Although we found no evidence for a correlation between the strength of hexadirectional modulation and task performance across controls ($r=0.15$, $p=0.49$), we did find a significant relationship between the consistency of the grid orientation across blocks and task performance ($r=-0.52$, $p=0.013$; Fig. 3H). This indicates that control participants with grid patterns that were more consistent across task blocks tended to more accurately remember object locations in the VR environments. Within the patient group, we found no evidence for differences in task performance, medication, or symptom severity between participants with (8/17) and without (9/17) hexadirectional modulation of theta power in the same ROI (all $p>0.22$).

Discussion

Our results demonstrate that people with schizophrenia show worse spatial memory and less movement-related theta power during a virtual spatial navigation task than a matched control group. They also lack the hexadirectional modulation of theta power in right entorhinal cortex observed in the control group, which is consistent with the presence of stable grid cell firing patterns. Importantly, the stability of grid orientation across task blocks in the control population correlated positively with their performance in the spatial memory task, suggesting a functional relationship between grid firing patterns and spatial memory. This is the first demonstration of hexadirectional theta modulation in MEG, building on previous studies showing similar patterns in BOLD signal throughout the default mode network[26,37], in high frequency activity from the anterior temporal lobe in both MEG and intracranial EEG recordings[48], and in entorhinal theta power from intracranial EEG recordings[35,36]. Crucially, however, the relationship between grid cell activity at the neural level, network level modulations of theta or high frequency power in the local field potential or in MEG, and the BOLD signal measured using fMRI are not clear, and merits further attention.

Previous studies have reported impaired spatial navigation associated with hippocampal anomalies in schizophrenia[15-19]. In particular, people with schizophrenia are selectively impaired in spatial navigation strategies based on cognitive mapping, rather than single-landmark (response-based) strategies[18,19]. Schizophrenia is also associated with impairments in associative inference and acquisition of relational knowledge[1,49-51], in which the hippocampal formation - and grid cells in particular - are thought to play a key role[27]. Our findings therefore suggest that dysfunctional grid coding may underlie atypical inference and poor acquisition of relational knowledge in schizophrenia. Grid firing patterns may be supported by attractor network dynamics[52], and attractor states are thought to be more unstable in schizophrenia[53,54], potentially due to reduced α5-GABA-A receptor density in the MTL[55]. We speculate that this may increase reliance on striatal learning mechanisms, making inferences more dependent on individual landmarks (or, perhaps, events) than structured relational knowledge of the world.

We note that movement related increases in theta power and the hexadirectional modulation of theta power by movement direction appear to be related but distinct phenomena. First, we found no correlation between movement related theta power and the strength of hexadirectional

modulation across our control group. Second, movement related theta power increases at the sensor level are most prominent over left frontal regions, while the hexadirectional modulation of theta power by movement direction is restricted to right entorhinal cortex. In contrast, we found no evidence for hexadirectional theta modulation in an anatomically-defined left entorhinal cortex ROI, although we are reluctant to over interpret this absence of evidence, given previous observations of grid cells[21] and the hexadirectional modulation of theta power in bilateral entorhinal cortex[35,36].

In summary, in healthy volunteers performing a virtual spatial navigation task, we have shown grid-like modulation of MEG theta power localised to the right entorhinal cortex whose consistency of orientation across virtual environments correlates with spatial memory performance. Relative to this baseline, we have shown that people with a diagnosis of schizophrenia have impaired spatial memory performance, reduced movement-related theta oscillations and disrupted grid-like modulation of theta power. This extends previous work showing structural and functional impairment of the hippocampal formation in schizophrenia and selective deficits of hippocampus-dependent strategies in spatial navigation. Future studies could address a possible role of grid cell populations in impaired structural knowledge and inference in schizophrenia.

Acknowledgements

The authors are grateful to Faith Borgan, Ilinca Angelescu, Andrew Watson, Nicholas Green, and Lynis Lewis (Noclor) for their help in recruiting participants with schizophrenia, and also to the imaging support staff at the Wellcome Centre for Human Neuroimaging, in particular Daniel Bates and David Bradbury.

Funding

LC is supported by the Leverhulme Doctoral Training Programme for the Ecological Study of the Brain (DS-2017-026). RAA is an MRC Skills Development Fellow (MR/S007806/1) and has also been supported by the Academy of Medical Sciences (AMS-SGCL13-Adams), the

National Institute of Health Research (CL-2013-18-003), and the NIHR UCLH Biomedical Research Centre. NB is a Wellcome Principal Research Fellow (222457/Z/21/Z) and has also been supported by a European Research Council advanced grant NEUROMEM (ERC-2015-AdG, 694779).

Competing interests

The authors report no competing interests.

Supplementary material

Supplementary material is available at *Brain* online.

References

[1] Adams RA, Bush D, Zheng F *et al.* Impaired theta phase coupling underlies frontotemporal dysconnectivity in schizophrenia. *Brain.* 2020; 143(4): 1261-1277.

[2] Harrison PJ. The hippocampus in schizophrenia: a review of the neuropathological evidence and its pathophysiological implications. *Psychopharmacology (Berl).* 2004; 174(1): 151-162.

[3] Heckers S Neuroimaging studies of the hippocampus in schizophrenia. *Hippocampus.* 2001; 11(5): 520-528.

[4] Heckers S, Konradi C. Hippocampal neurons in schizophrenia. *J Neural Transm (Vienna).* 2002; 109(5-6): 891-905.

[5] Lieberman JA, Girgis RR, Brucato G, Moore H, Provenzano F, Kegeles L *et al.* Hippocampal dysfunction in the pathophysiology of schizophrenia: a selective review and hypothesis for early detection and intervention. *Molecular Psychiatry.* 2018; 23(8): 1764-1772.

[6] Baiano M, Perlini C, Rambaldelli G, Cerini R, Dusi N, Bellani M *et al.* Decreased entorhinal cortex volumes in schizophrenia. *Schizophr Res.* 2008; 102(1-3): 171-180.

[7] Prasad KM, Patel AR, Muddasani S, Sweeney J, Keshavan MS. The entorhinal cortex in first-episode psychotic disorders: a structural magnetic resonance imaging study. *Am J Psychiatry.* 2004; 161(9): 1612-1619.

[8] Roalf DR, Quarmley M, Calkins ME, Satterthwaite TD, Ruparel K, Elliott MA *et al.* Temporal Lobe Volume Decrements in Psychosis Spectrum Youths. *Schizophr Bull.* 2016; 43(3): 601-610.

[9] Dickerson DD, Wolff AR, Bilkey DK. Abnormal long-range neural synchrony in a maternal immune activation animal model of schizophrenia. *J Neurosci.* 2010; 30(37): 12424-12431.

[10] Ellison-Wright I, Bullmore E. Meta-analysis of diffusion tensor imaging studies in schizophrenia. *Schizophr Res.* 2009; 108(1-3): 3-10.

[11] Sigurdsson T, Stark KL, Karayiorgou M, Gogos JA, Gordon JA. Impaired hippocampal-prefrontal synchrony in a genetic mouse model of schizophrenia. *Nature.* 2010; 464(7289): 763-767.

[12] Weinberger DR, Berman KF, Suddath R, Torrey EF. Evidence of dysfunction of a prefrontal-limbic network in schizophrenia: a magnetic resonance imaging and regional cerebral blood flow study of discordant monozygotic twins. *Am J Psychiatry.* 1992; 149(7): 890-897.

[13] Bird CM, Burgess N. The hippocampus and memory: insights from spatial processing. *Nat Rev Neurosci.* 2008; 9(3): 182-194.

[14] Burgess N, Maguire EA, O'Keefe J. The Human Hippocampus and Spatial and Episodic Memory. *Neuron.* 2002; 35(4): 625-641.

[15] Ledoux AA, Boyer P, Phillips JL, Labelle A, Smith A, Bohbot VD. Structural hippocampal anomalies in a schizophrenia population correlate with navigation performance on a wayfinding task. *Front Behav Neurosci.* 2014; *8*: 88.

[16] Mohammadi A, Hesami E, Kargar M, Shams J. Detecting allocentric and egocentric navigation deficits in patients with schizophrenia and bipolar disorder using virtual reality. *Neuropsychol Rehabil.* 2018; 28(3): 398-415.

[17] Salgado-Pineda P, Landin-Romero R, Portillo F, Bosque C, Pomes A, Spanlang B *et al.* Examining hippocampal function in schizophrenia using a virtual reality spatial navigation task. *Schizophr Res.* 2016; 172(1-3), 86-93.

[18] Wilkins LK, Girard TA, Christensen BK, King J, Kiang M, Bohbot VD. Spontaneous spatial navigation circuitry in schizophrenia spectrum disorders. *Psychiatry Res.* 2019; 278: 125-128.

[19] Wilkins LK, Girard TA, Konishi K, King M, Herdman KA, King J *et al.* Selective deficit in spatial memory strategies contrast to intact response strategies in patients with schizophrenia spectrum disorders tested in a virtual navigation task. *Hippocampus.* 2013; 23(11): 1015-1024.

[20] Hafting T, Fyhn M, Molden S, Moser M-B, Moser EI. Microstructure of a spatial map in the entorhinal cortex. *Nature.* 2005; 436(7052): 801-806.

[21] Jacobs J, Weidemann CT, Miller JF, Solway A, Burke JF, Wei X-X *et al.* Direct recordings of grid-like neuronal activity in human spatial navigation. *Nat Neurosci.* 201; 16(9): 1188-1190.

[22] Bush D, Barry C, Manson D, Burgess N. Using Grid Cells for Navigation. *Neuron.* 2015; 87(3): 507-520.

[23] Gil M, Ancau M, Schlesiger MI *et al.* Impaired path integration in mice with disrupted grid cell firing. *Nat Neurosci.* 2018; 21**:** 81–91.

[24] Tennant SA, Fischer L, Garden DLF, Gerlei KZ, Martinez-Gonzalez C, McClure C *et al.* Stellate Cells in the Medial Entorhinal Cortex Are Required for Spatial Learning. *Cell Rep.* 2018; 22(5): 1313-1324.

[25] Aronov D, Nevers R, Tank DW. Mapping of a non-spatial dimension by the hippocampal-entorhinal circuit. *Nature.* 2017; 543(7647): 719-722.

[26] Constantinescu AO, O'Reilly JX, Behrens TEJ. Organizing conceptual knowledge in humans with a gridlike code. *Science.* 2016; 352(6292): 1464-1468.

[27] Behrens TEJ, Muller TH, Whittington JCR, Mark S, Baram AB, Stachenfeld KL *et al.* What Is a Cognitive Map? Organizing Knowledge for Flexible Behavior. *Neuron.* 2018; 100(2): 490-509.

[28] Brandon MP, Bogaard AR, Libby CP, Connerney MA, Gupta K, Hasselmo ME. Reduction of theta rhythm dissociates grid cell spatial periodicity from directional tuning. *Science.* 2011; 332(6029): 595-599.

[29] Koenig J, Linder AN, Leutgeb JK, Leutgeb S. The spatial periodicity of grid cells is not sustained during reduced theta oscillations. *Science.* 2011; 332(6029): 592-595.

[30] Winter SS, Mehlman ML, Clark BJ, Taube JS. Passive Transport Disrupts Grid Signals in the Parahippocampal Cortex. *Curr Biol.* 2015; 25(19): 2493-2502.

[31] Aghajan Z, Schuette P, Fields TA, Tran ME, Siddiqui SM, Hasulak NR *et al*. Theta Oscillations in the Human Medial Temporal Lobe during Real-World Ambulatory Movement. *Curr Biol.* 2017; 27(24): 3743-3751.

[32] Bohbot VD, Copara MS, Gotman J, Ekstrom AD. Low-frequency theta oscillations in the human hippocampus during real-world and virtual navigation. *Nat Commun*. 2017; 8: 14415.

[33] Kahana MJ, Sekuler R, Caplan JB, Kirschen M, Madsen JR. Human theta oscillations exhibit task dependence during virtual maze navigation. *Nature.* 1999; 399(6738): 781-4.

[34] Bush D, Bisby JA, Bird CM, Gollwitzer S, Rodionov R, Diehl B *et al.* Human hippocampal theta power indicates movement onset and distance travelled. *Proc Natl Acad Sci U S A.* 2017; 114(46): 12297-12302.

[35] Chen D, Kunz L, Wang W, Zhang H, Wang W-X, Schulze-Bonhage A *et al.* Hexadirectional Modulation of theta Power in Human Entorhinal Cortex during Spatial Navigation. *Curr Biol.* 2018; 28(20): 3310-3315.

[36] Maidenbaum S, Miller J, Stein JM, Jacobs J. Grid-like hexadirectional modulation of human entorhinal theta oscillations. *Proc Natl Acad Sci U S A.* 2018; 115(42): 10798-10803.

[37] Doeller CF, Barry C, Burgess N. Evidence for grid cells in a human memory network. *Nature.* 2010; 463(7281): 657-661.

[38] Kaplan R, Bush D, Bonnefond M, Bandettini PA, Barnes GR, Doeller CF *et al.* Medial prefrontal theta phase coupling during spatial memory retrieval. *Hippocampus.* 2014; 24(6): 656-665.

[39] Kaplan R, Doeller CF, Barnes GR, Litvak V, Düzel E, Bandettini PA *et al.* Movement-related theta rhythm in humans: coordinating self-directed hippocampal learning. *PLoS Biol.* 2012; 10(2): e1001267.

[40] Kay SR, Fiszbein A, Opler LA. The positive and negative syndrome scale (PANSS) for schizophrenia. *Schizophr Bull.* 1987; 13(2): 261-276.

[41] First MB, Williams JB, Spitzer RL, Gibbon M. Structured clinical interview for DSM-IV-TR axis I disorders, clinical trials version (SCID-CT). *New York: Biometrics Research, New York State Psychiatric Institute*. 2007

[42] Doeller CF, King JA, Burgess N. Parallel striatal and hippocampal systems for landmarks and boundaries in spatial memory. *Proc Natl Acad Sci U S A.* 2008; 105(15): 5915-5920.

[43] Litvak V, Mattout J, Kiebel S, Phillips C, Henson R, Kilner J et al. EEG and MEG Data Analysis in SPM8. *Computational Intelligence and Neuroscience.* 2011; 852961.

[44] Oostenveld R, Fries P, Maris E, Schoffelen JM. FieldTrip: Open source software for advanced analysis of MEG, EEG, and invasive electrophysiological data. *Computational Intelligence and Neuroscience.* 2011; 156869.

[45] Delorme A, Makeig S. EEGLAB: an open source toolbox for analysis of single-trial EEG dynamics including independent component analysis. *J Neurosci Methods.* 2004; 134(1): 9-21.

[46] Barnes GR, Hillebrand A. Statistical flattening of MEG beamformer images. *Human Brain Mapping.* 2003; 18(1): 1-12.

[47] Amunts K, Mohlberg H, Bludau S, Zilles K. Julich-Brain: A 3D probabilistic atlas of the human brain's cytoarchitecture. *Science.* 2020; 369(6506): 988-992.

[48] Staudigl T, Leszczynski M, Jacobs J, Sheth SA, Schroeder CE, Jensen O *et al.* Hexadirectional Modulation of High-Frequency Electrophysiological Activity in the

Human Anterior Medial Temporal Lobe Maps Visual Space. *Curr Biol.* 2018; 28(20): 3325-3329.

[49] Armstrong K, Avery S, Blackford JU, Woodward N, Heckers S. Impaired associative inference in the early stage of psychosis. *Schizophr Res.* 2018; 202: 86-90.

[50] Armstrong K, Kose S, Williams L, Woolard A, Heckers S. Impaired associative inference in patients with schizophrenia. *Schizophr Bull.* 2012; 38(3): 622-629.

[51] Armstrong K, Williams LE, Heckers S. Revised associative inference paradigm confirms relational memory impairment in schizophrenia. *Neuropsychology.* 2012; 26(4), 451-458.

[52] McNaughton BL, Battaglia FP, Jensen O, Moser EI, Moser M-B. Path integration and the neural basis of the 'cognitive map'. *Nat Rev Neurosci.* 2006; 7(8): 663-78.

[53] Adams RA, Napier G, Roiser JP, Mathys C, Gilleen J. Attractor-like dynamics in belief updating in schizophrenia. *J Neurosci.* 2018; 38(44): 9471-9485.

[54] Hamm JP, Peterka DS, Gogos JA, Yuste R. Altered Cortical Ensembles in Mouse Models of Schizophrenia. *Neuron.* 2017; 94(1): 153-167.

[55] Marques TR et al. GABA-A receptor differences in schizophrenia: a positron emission tomography study using [11C]Ro154513. *Mol Psychiatry.* 2021; 26(6): 2616-2625.

Figure legends

Figure 1 Spatial Memory Task. A) Schematic. Participants navigate through the environment and make responses using a button box. During encoding, they are asked to remember the locations of four objects (one object being visible in each trial). During retrieval, a fixation cross on a grey screen is followed by an image of one object (cue period). The participants are then asked to navigate from a random start location to the retrieved location of that object and make a response. During navigation, the object image remains visible in the top left corner of the screen. Following a response, the object appears in its correct location to provide feedback. The next trial begins when the participants collide with the object. **B)** Performance, quantified as the inverse of the average distance between remembered and actual object locations, for controls (in blue) and patients (in red). Each red line indicates the median, box edges the 25^{th} and 75^{th} percentiles, whiskers extend to the most extreme datapoints not considered to be outliers (defined as values more than 1.5 times above or below the 75^{th} and 25^{th} percentile, respectively), and outliers are plotted individually. Spatial memory accuracy was significantly higher in the control group.

Figure 2 Movement-related 4-10Hz theta power increases in controls and patients. A) Power spectra showing normalised power during movement onset epochs (i.e. [-0.5 0.5] s around the onset of ≥1 s translational movements that were preceded by ≥1 s immobility), baseline corrected by average power during stationary periods (i.e. [0 1] s around the onset of ≥2 s periods of immobility) for controls (in blue) and patients (in red, shading indicates standard error). The grey bar delineates the 4-10 Hz theta band. **B)** Time-frequency spectrograms showing normalised power during movement onset, baseline corrected by average power during stationary periods. Controls show a marked increase in theta power beginning ~0.5 s prior to movement onset that is reduced in patients. **C)** Scalp plots of normalised 4-10 Hz theta power during movement onset epochs, baseline corrected by average theta power during stationary periods for controls, patients, and for the contrast between groups. Highlighted channels show significant positive power differences at a threshold of $p<0.01$ (uncorrected).

Figure 3 Modulation of oscillatory power by movement direction in right entorhinal cortex. **A)** Regions showing significant hexadirectional modulation of 4-10Hz theta power at the whole brain level. Only one cluster in right entorhinal cortex (peak at [18 -22 -44], Z=4.05) passes our significance threshold of $p<0.05$ FWE corrected (image shown at $p<0.005$ uncorrected, for display purposes). **B)** Image of the anatomically defined right entorhinal cortex region of interest (ROI). **C)** Strength of hexadirectional theta modulation inside the ROI for controls and patients, with 19/23 controls (82.6%) and 8/17 patients (47.1%) showing a positive beta coefficient. **D)** Difference in theta power between on vs off axis movement inside the ROI for controls and patients, with 19/23 controls (82.6%) and 7/17 patients (41.2%) showing greater on vs off axis theta power. **E)** Difference in the percentage of movement samples that occurred during on vs off axis movement for controls and patients. **F)** Theta modulation by 4-8 fold movement direction inside the ROI for controls. **G)** Strength of hexadirectional modulation of delta (2-4Hz), theta (4-10Hz), alpha (12-20Hz), beta (20-35Hz) and gamma (40-70Hz) frequency bands inside the ROI for controls. **H)** Correlation between performance, quantified as the inverse of the average distance between remembered and actual object locations, and grid (in)stability across task blocks for controls. Each red line indicates the median, box edges the 25^{th} and 75^{th} percentiles, whiskers extend to the most extreme datapoints not considered to be outliers (defined as values more than 1.5 times above or below the 75^{th} and 25^{th} percentile, respectively), and outliers are plotted individually.

Table 1 Number of movement and stationary periods (or 'epochs') in controls and patients

	Total movement epochs (mean ± SD)	Bad movement trials (mean ± SD, %)	Included movement trials (mean ± SD, range)	Stationary epochs (mean ± SD)	Bad stationary trials (mean ± SD, %)	Included stationary trials (mean ± SD, range)
CONTROLS	122.6 ± 35.3	3.39 ± 4.22%	119.0 ± 36.4, 61–192	241.7 ± 75.5	3.03 ± 3.92%	234.9 ± 76.6, 110–43
PATIENTS	142.8 ± 45.3	6.95 ± 6.89%	133.5 ± 45.8, 38–246	278.4 ± 82.5	5.91 ± 5.11%	262.9 ± 81.4, 86–408

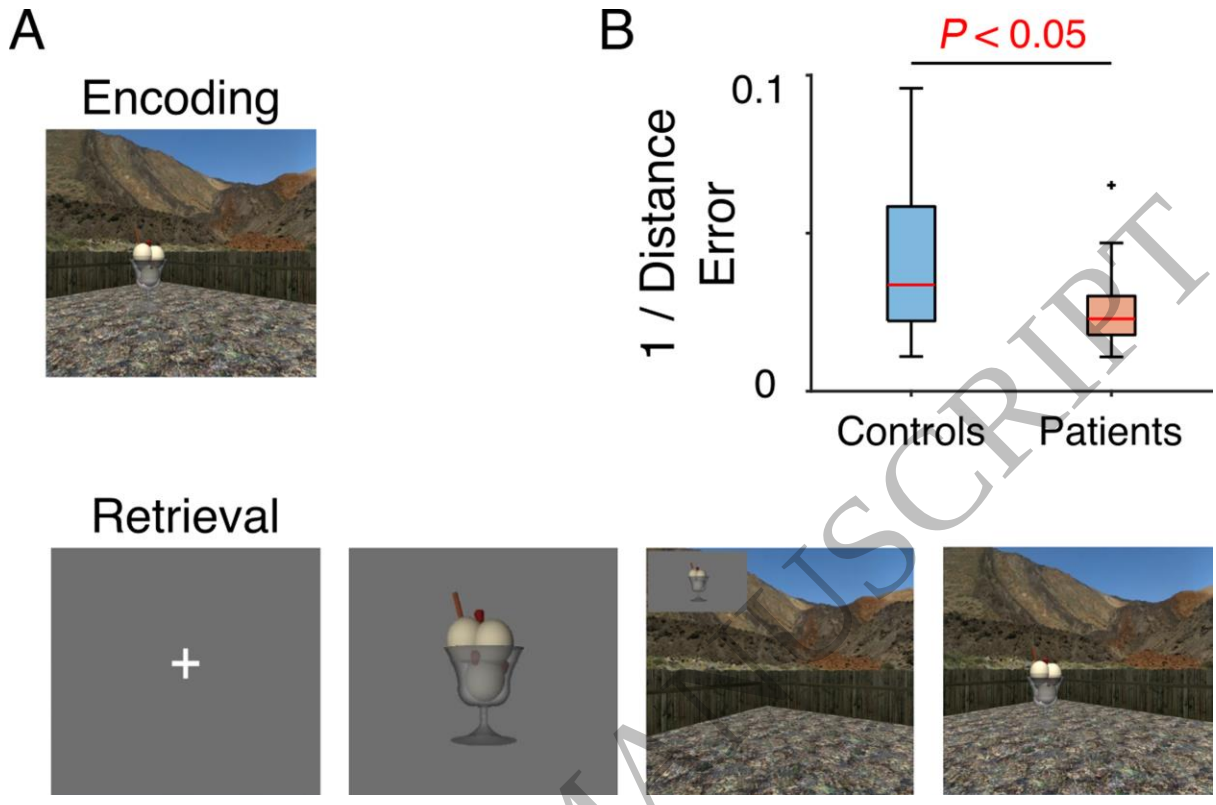

Figure 1
159x104 mm (x DPI)

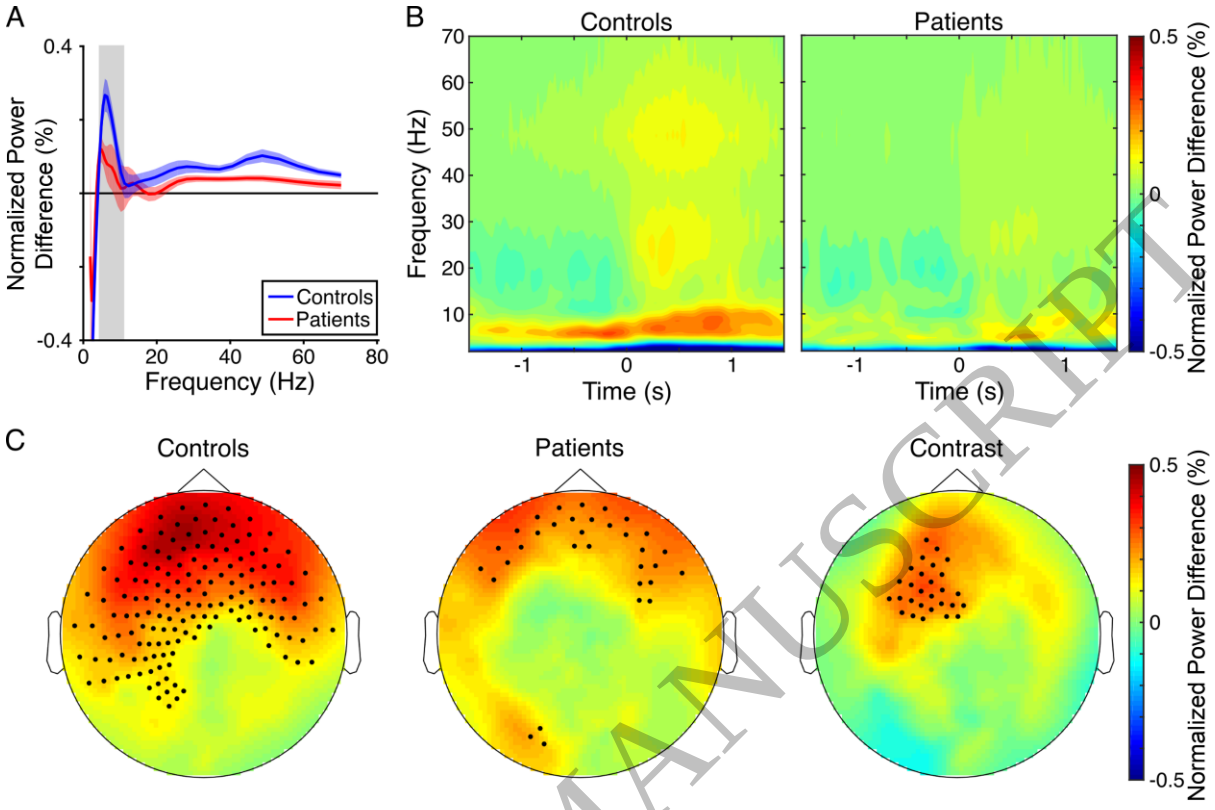

Figure 2
159x105 mm (x DPI)

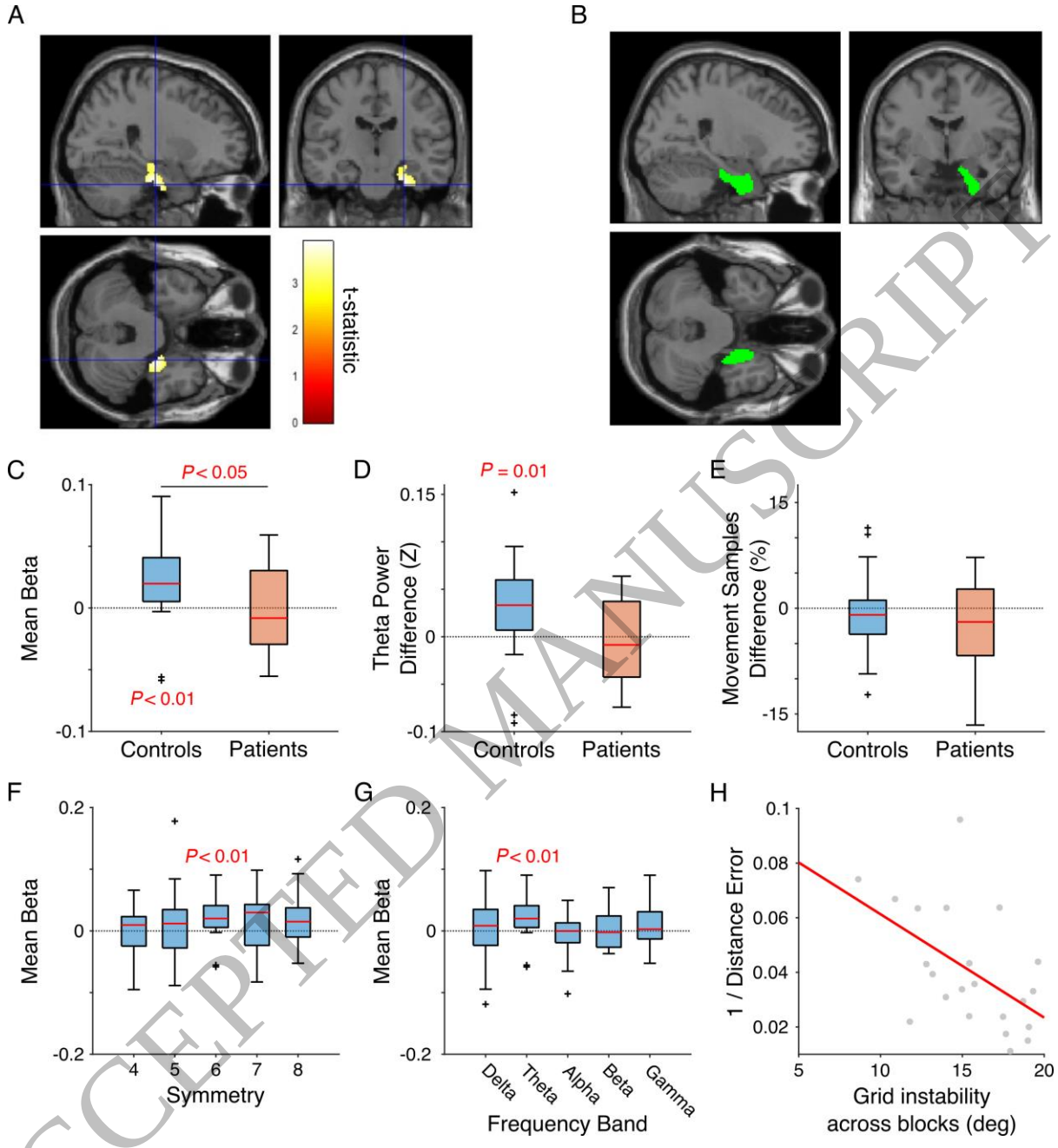

Figure 3
159x172 mm (x DPI)